Mini focus on bioresorbable scaffolds

Preclinical investigation of neoatherosclerosis in magnesium-based bioresorbable scaffolds versus thick-strut drug-eluting stents

Philipp Nicol[1], MD; Anna Bulin[1], DVM, MD; Maria Isabel Castellanos[1,2], PhD; Magdalena Stöger[1], MS; Simone Obermeier[1], MS; Jonas Lewerich[1], MS; Tobias Lenz[1], MD; Petra Hoppmann[2,3], MD; Christine Baumgartner[4], DVM; Johannes Fischer[4], DVM; Katja Steiger[5], DVM; Michael Haude[6], MD; Michael Joner[1,2]*, MD

1. Deutsches Herzzentrum München and Deutsches Zentrum für Herz-Kreislaufforschung e.V., Munich, Germany; 2. DZHK (German Centre for Cardiovascular Research), partner site Munich Heart Alliance, Munich, Germany; 3. Klinik und Poliklinik für Innere Medizin I, Klinikum rechts der Isar, Technische Universität München, Munich, Germany; 4. Zentrum für präklinische Forschung, Technische Universität München, Munich, Germany; 5. Institut für Pathologie, Technische Universität München, Munich, Germany; 6. Städtische Kliniken Neuss, Lukaskrankenhaus GmbH, Neuss, Germany

P. Nicol and A. Bulin contributed equally to this manuscript.

This paper also includes supplementary data published online at: https://eurointervention.pcronline.com/doi/10.4244/EIJ-D-19-00747

Abstract

Aims: Neoatherosclerosis is a frequent finding after implantation of permanent metallic stents. Bioresorbable scaffolds (BRS) are considered to reduce the incidence of neoatherosclerosis owing to their dissolution and consequent vascular restoration. The aim of this study was to evaluate the formation of neoatherosclerosis between magnesium-based BRS and thick-strut metallic drug-eluting stents (DES) in a rabbit model of neoatherosclerosis and in proportion to the effect of high-dose statin medication.

Methods and results: Fully bioresorbable magnesium scaffolds (BRS, n=45) and thick-strut permanent metallic DES of equivalent geometry and design (n=45) were implanted into the iliac arteries of New Zealand White rabbits (n=45) following endothelial balloon injury and exposure to a cholesterol diet. Endothelialisation was assessed in 12 animals after 35 days using scanning electron microscopy (SEM), showing significantly enhanced re-endothelialisation above struts in the BRS (n=13) compared to DES (n=10). Eleven (11) animals were terminated for baseline assessment after 91 days while the remaining 22 animals were randomised to receive high-dose statin treatment (3 mg/kg) or placebo. BRS-treated vessels showed a significant reduction in foam cell infiltration as a sign of early neoatherosclerosis by histology and OCT when compared to thick-strut DES-treated vessels. Statin treatment resulted in significant reduction of foam cell infiltration in BRS and DES by histology.

Conclusions: Our findings suggest reduced neoatherosclerosis formation in magnesium-based BRS relative to thick-strut DES. High-dose statin treatment may be a promising measure to reduce neoatherosclerosis progression, both on its own and in synergy with site-targeted device-based treatment.

*Corresponding author: German Heart Center Munich, Lazarettstrasse 36, 80636 Munich, Germany.
E-mail: joner@dhm.mhn.de

Abbreviations

atm	atmosphere
BRS	bioresorbable scaffold(s)
CI	confidence interval
DAH	delayed arterial healing
DES	drug-eluting stent
GEE	generalised estimating equation(s)
MMA	methyl methacrylate
OCT	optical coherence tomography
PLLA	poly-L-lactic acid
SEM	scanning electron microscopy

Introduction

Atherothrombotic cardiovascular disease is the leading cause of morbidity and mortality worldwide[1]. In patients with obstructive coronary artery disease, percutaneous angioplasty and stenting is the first treatment of choice[2]. However, while a considerable reduction of in-stent restenosis was achieved with the introduction of drug-eluting stents (DES), the undoubted success of this technology is delivered at the collateral cost of delayed arterial healing (DAH), a pathophysiological entity which underlies a spectrum of adverse clinical events[3,4]. In-stent neoatherosclerosis has recently been recognised as an important disease entity in patients after stent implantation, representing an additional manifestation of atherosclerotic disease found in nascent neointimal tissue after stent implantation[4].

Bioresorbable scaffolds (BRS) have recently been introduced into clinical practice. It has been proposed that their transient presence in the coronary artery may mitigate neoatherosclerosis formation. While first-generation polymer-based BRS are hampered by inherent shortcomings such as excessive strut thickness and slow degradation profile[5], newer device iterations are targeted to address these limitations and provide a more rapid vascular restoration[6].

Furthermore, pharmacological targeting of risk factors such as hyperlipidaemia using high-dose statin treatment significantly decreased mortality in secondary prevention after manifestation of coronary artery disease[7]. Consequently, we aimed to investigate whether site-targeted treatment using magnesium-based BRS technology mitigates neoatherosclerosis formation in a novel hypercholesterolaemic animal model when compared to local control therapy with permanent metallic DES. It was another goal of this study to investigate the effect of BRS versus DES progression of neoatherosclerosis in proportion to systemic treatment with atorvastatin compared to placebo. The study flow is shown in **Figure 1**.

Methods

Please refer to **Supplementary Appendix 1** for details regarding materials and methods.

Results

Of the 33 rabbits included in the histology study, two animals died of cholesterol-induced liver failure. Two additional animals had to be excluded from analysis due to total thrombotic occlusion of a stented vessel (one rabbit with thrombosis in BRS, one with thrombosis in DES). Accordingly, a total of nine animals were available in group 1 (day 91). A total of 10 animals each remained in groups 2 and 3, respectively, until day 161.

Serum levels of cholesterol differed significantly between groups with an area under the curve (AUC) of 3608.97 in group 1 (baseline) and an AUC of 3319.28 in group 2 (statin treatment) versus 4016.92 in group 3 (placebo treatment; p=0.02) **(Supplementary Figure 1)**.

The results of group 1 are shown in **Supplementary Table 1**, **Supplementary Table 2**, and **Supplementary Appendix 2**. There was no early mortality in the 12 rabbits assigned to scanning electron microscopy (SEM) assessment of endothelialisation.
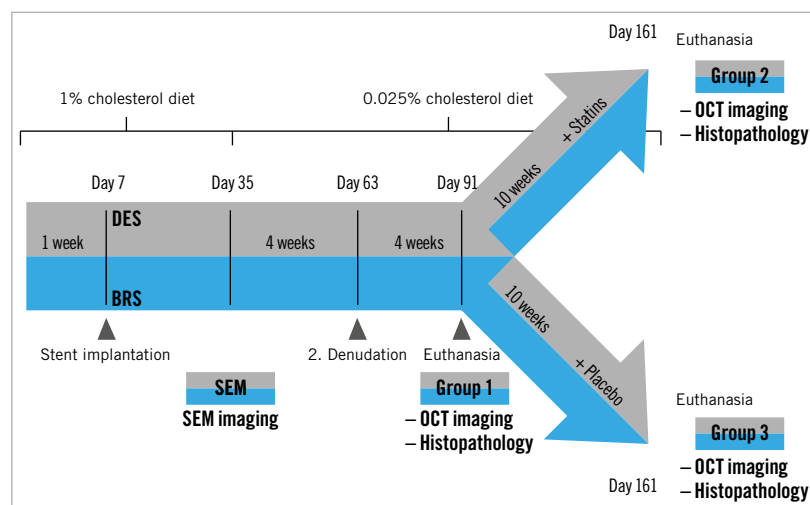

Figure 1. *Study flow chart. All animals received BRS and DES in the iliac arteries seven days after the start of a 1% cholesterol diet and were switched to a low-dose cholesterol diet on day 35. Repeat balloon denudation was performed on day 63. On day 91, animals of group 1 were terminated while the remaining animals were randomised to statin treatment or placebo. The animals in groups 2 and 3 were euthanised on day 161.*

NEOATHEROSCLEROSIS SCORING BY HISTOLOGY

BRS showed a significantly lower estimated score of foamy macrophage infiltration compared to DES (score 1.16 [1.12, 1.21] vs 1.53 [1.41, 1.65]; mean reduction −0.361; p<0.0001) **(Figure 2A)**. A neointimal foam cell score was additionally assigned to each quadrant of histological cross-sections, treated as a categorical variable and compared among treatment groups (BRS vs DES). Each quadrant showed significant differences based on Pearson's chi square, with a higher percentage of foam cell score 2-4 in DES relative to BRS (p<0.05 for all quadrants).

Statin treatment resulted in a significant reduction of foamy macrophage infiltration relative to placebo (score 1.23 [1.14, 1.32] vs 1.45 [1.36, 1.54]; mean reduction −0.221; p=0.001) **(Figure 2B, Table 1)**. Variability of scoring was assessed by calculating the intraclass and interclass correlation coefficient (0.98 and 0.90, respectively).

There was significant statistical interaction (p=0.005) among stent types and treatment allocation to statin versus placebo. **Figure 3** shows representative co-registration of haematoxylin and eosin (H&E)-stained histological slides and optical coherence tomography (OCT) frames in both BRS and DES.
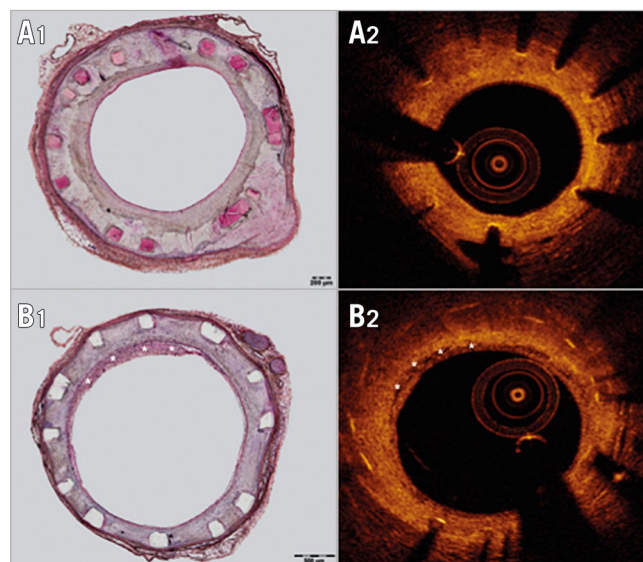

Figure 3. *Comparison and co-registration of BRS and DES. A) Sections stained for H&E (A1) with corresponding OCT frame (A2) in a BRS-treated vessel. B) Sections stained for H&E (B1) with corresponding OCT frame (B2) in a DES-treated vessel. Asterisks (*) indicate foamy macrophage infiltration.*
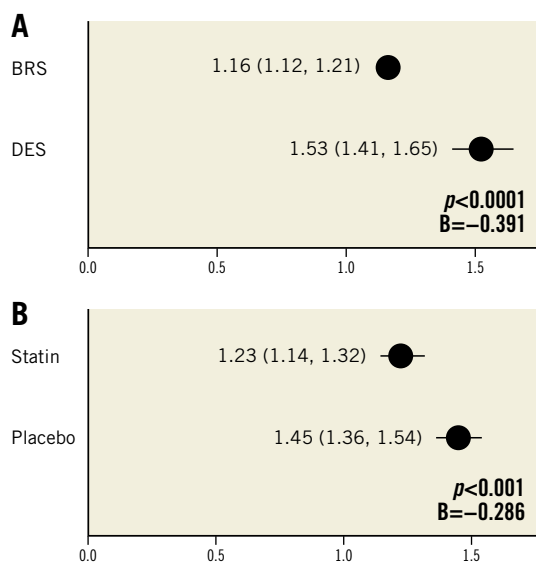
NEOATHEROSCLEROSIS SCORING BY OCT

An overview of the results is presented in **Table 2**. BRS showed a significantly lower estimated score of macrophage infiltration by OCT compared to DES (score 1.20 [1.08, 1.34] vs 2.09 [1.83, 2.39]; mean reduction −0.886; p<0.0001) **(Figure 4A)**. There was no statistically significant difference in animals receiving statin treatment relative to placebo by OCT (score 1.57 [1.32, 1.87] vs 1.60 [1.44, 1.77]; mean reduction −0.26; p=0.873) **(Figure 4B)**. Variability of scoring was assessed by calculating the intraclass and interclass correlation coefficient (0.74 and 0.69, respectively).

MORPHOMETRIC ANALYSIS IN OCT AND HISTOPATHOLOGY

Morphometric assessment revealed significantly greater neointimal area in BRS relative to DES by OCT (1.86 mm^2 vs 1.32 mm^2; mean difference +0.541 in BRS; p<0.0001) and histology (3.22 mm^2

Figure 2. *Neoatherosclerosis in histological sections (n=20 rabbits). Estimated mean neoatherosclerosis score derived by generalised estimating equations (lower/upper CI) shows a significant reduction of foamy macrophage infiltration in BRS as compared to DES (A) and statin-treated animals versus placebo (B).*

Table 1. Results of histopathological analysis of groups 2 and 3 after 161 days (n=10 rabbits for each group).

		Neoatherosclerosis score					% Stenosis				
		Mean	Lower 95% CI	Upper 95% CI	*p*-value	B-value	Mean	Lower 95% CI	Upper 95% CI	*p*-value	B-value
Treatment	BRS, n=10	1.16	1.12	1.21	0.0001*	−0.391	68.64	64.82	72.69	0.0001*	0.679
	DES, n=10	1.53	1.41	1.65			35.53	32.33	39.04		
Group	Statin, n=10	1.23	1.14	1.32	0.001*	−0.286	49.33	44.22	55.03	0.977	0.018
	Placebo, n=10	1.45	1.36	1.54			49.43	45.39	53.84		
p for interaction		0.005*					0.577				

Values are presented as estimated means with upper and lower 95% CI. A *p*<0.05 was considered statistically significant (*). Wilcoxon Kruskal-Wallis (non-parametric) or ANOVA (parametric) was applied.
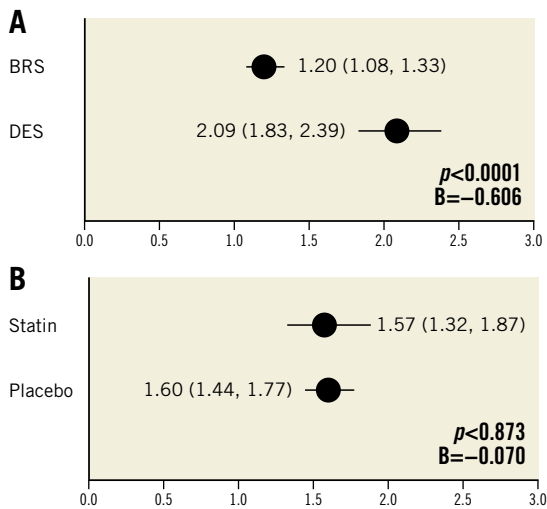
Figure 4. *Neoatherosclerosis in OCT (n=20 rabbits). Estimated mean neoatherosclerosis score derived by generalised estimating equations (lower/upper CI) assessed in OCT imaging shows a significant reduction of foamy macrophage infiltration in BRS as compared to DES (A) and a non-significant reduction in the statin-treated versus the placebo group (B).*

Figure 5. *Percentage stenosis comparing BRS versus DES in OCT and histopathology (n=20 rabbits). A) Estimated mean percentage stenosis derived by generalised estimating equations (lower/upper CI) as assessed by morphometrical analysis of histology in both BRS and DES. B) Estimated mean percentage stenosis derived by generalised estimating equations (lower/upper CI) as assessed by OCT imaging in both BRS and DES.*

vs 2.27 mm²; mean difference +0.948 in BRS; p<0.0001). This resulted in increased percentage stenosis in BRS-treated arteries relative to DES – 47% in BRS vs 21.8% in DES (p<0.0001) in OCT analysis **(Table 2)** and 68.6% vs 35.5% (p<0.0001) in histological analysis **(Table 1, Figure 5)**.

HISTOLOGICAL AND IMMUNOHISTOLOGICAL STAINING

Neointimal tissue consisted of smooth muscle cells in a proteoglycan-rich matrix. Inflammation of neointimal tissue, consisting of lymphocytes and for the largest part neutrophilic granulocytes, was generally mild to moderate with a tendency towards greater inflammation in BRS relative to DES (inflammation score: 1.53 in BRS vs 1.24 in DES, p=0.106). Cholesterol crystals were frequently observed in deeper tissue layers in both BRS and DES. Giant cells were mainly observed within the peri-strut regions (% giant cells: 9.33% in BRS vs 7.70% in DES, p=0.335). In segments stained for RAM11, macrophage infiltration was frequently
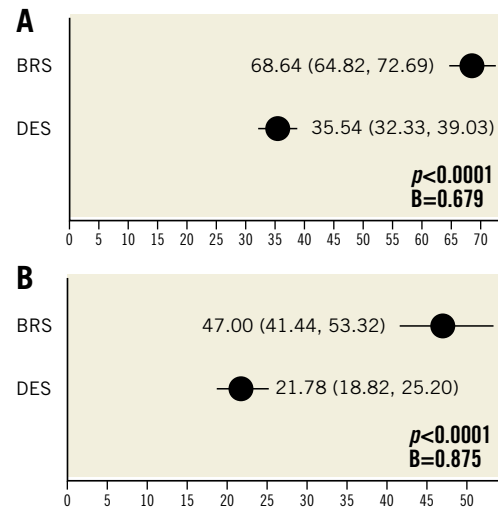
observed within the subintimal tissue in DES, while BRS showed scattered macrophages within the peri-strut tissue **(Figure 6)**. Additionally, staining against smooth muscle actin (SMA) showed formation of mature smooth muscle cells in BRS **(Figure 7A1, Figure 7A2)**, while DES did not show any positive staining for SMA **(Figure 7B1, Figure 7B2)**. For detailed results of histopathological assessment and morphometry in histology and OCT please refer to **Supplementary Table 3** and **Supplementary Table 4**.

ENDOTHELIAL CELL COVERAGE

Re-endothelialisation following catheter denudation and stenting was evaluated in 12 animals (n=13 BRS, n=10 DES) using SEM. Twenty-eight days following stent implantation (day 35), magnesium-based BRS showed significantly improved endothelial cell coverage above struts as compared to the 316L DES of equivalent design (91.7±20.2% vs 42.1±57.16%; p<0.001) **(Figure 8)**.

Table 2. Results of OCT analysis of groups 2 and 3 after 161 days (n=10 rabbits for each group).

|		Neoatherosclerosis score					% Stenosis				
		Mean	Lower 95% CI	Upper 95% CI	*p*-value	B-value	Mean	Lower 95% CI	Upper 95% CI	*p*-value	B-value
Treatment	BRS, n=10	1.20	1.08	1.34	0.0001*	−0.606	47.00	41.44	53.32	0.0001*	0.875
	DES, n=10	2.09	1.83	2.39			21.77	18.82	25.20		
Group	Statin, n=10	1.57	1.32	1.87	0.873	−0.070	32.31	27.03	38.61	0.857	0.125
	Placebo, n=10	1.60	1.44	1.77			31.68	28.14	35.67		
p for interaction		0.435					0.222				
Values are presented as estimated means with upper and lower 95% CI. A *p*<0.05 was considered statistically significant (*). Wilcoxon Kruskal-Wallis (non-parametric) or ANOVA (parametric) was applied.											
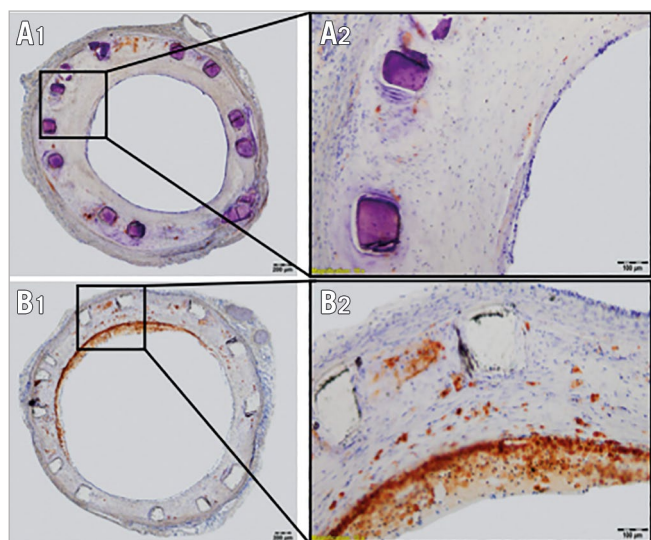
Figure 6. *RAM-11 staining in BRS and DES stented vessels. A) Overview of a RAM-11 stained section from a BRS (A1) with 40x magnification (A2). Sparse macrophage infiltration is detectable in peri-strut neointimal tissue. B) Overview of a RAM-11 stained section from a DES (B1), with 40x magnification (B2). Superficial foamy macrophage infiltration is visible in about 50% of the vessel circumference.*

Discussion

The current study investigated the differential magnitude of neoatherosclerosis formation after implantation of fully bioresorbable magnesium scaffolds and permanent metallic thick-strut DES of equivalent design and geometry in a novel animal model of in-stent neoatherosclerosis. Furthermore, it examined the impediment of neoatherosclerosis progression as a response to statin treatment relative to placebo in both stent types up to 161 days following study initiation. The most salient findings can be described as follows:

(i) Fully bioresorbable magnesium scaffolds showed enhanced endothelial cell coverage 28 days following stent implantation and decreased neointimal macrophage infiltration after 161 days when compared to permanent stainless steel thick-strut DES in a novel animal model of neoatherosclerosis.

(ii) There was significant statistical interaction between stent type and treatment allocation to atorvastatin versus placebo with regard to reduction of neointimal macrophage infiltration. Therefore, synergistic effects between local and systemic therapy are very likely.

(iii) Atorvastatin treatment as applied in the current study significantly reduced progression of neointimal macrophage infiltration in BRS and DES, which was confirmed by histopathological assessment.

(iv) Fully bioresorbable magnesium scaffolds showed significantly greater neointima burden as compared to thick-strut DES.

Development of neoatherosclerosis after stent implantation has been recognised as an important contributor to late stent failure. The implantation of DES was recently reported to result in earlier onset of neoatherosclerosis formation in *post mortem* autopsy and clinical imaging studies when compared to BMS[8,9]. Previous work has shown that DES exhibit markedly different neointimal composition with a higher amount of proteoglycan and fewer smooth muscle cells compared with BMS[10,11]. Notably, long-term follow-up of clinical trials investigating the comparative performance of early- and newer-generation DES reported a sustained increase in clinical events irrespective of the implanted stent type over time[12]. Short of a mechanistic explanation for this late increment in adverse events, preclinical and post-mortem autopsy studies have suggested delayed arterial healing with sustained inflammatory reaction, delayed endothelialisation and formation of in-stent neoatherosclerosis to be causative in the majority of cases. Consequently, bioresorbable scaffolds were introduced to overcome these inherent limitations associated with permanent metallic DES and proposed to reduce the burden of neoatherosclerosis owing to their temporary presence, where recovery of physiological vasomotion and normalisation of flow dynamics were suggested to impact favourably on plaque progression over time. However, those anticipated effects of BRS technology have not been proven in clinical practice.
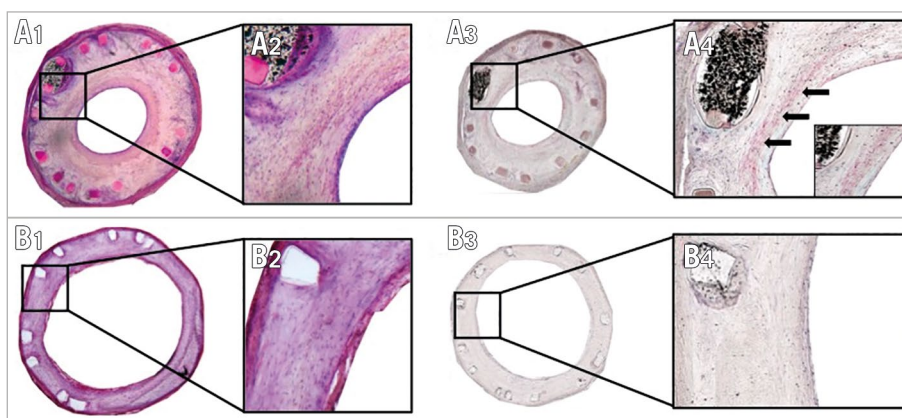
Figure 7. *SMA staining in BRS and DES stented vessel. H&E stained sections in BRS (A1) and DES (B1) show the presence of spindle-shaped cells, indicating smooth muscle cells (40x magnification in A2/B2). A3) & A4) SMA stained section from a BRS with 40x magnification. Positive areas reveal these cells to be mature smooth muscle cells (arrows). B3) & B4) SMA stained section from a DES. No positive areas are visible, indicating the absence of mature smooth muscle cells.*

Figure 8. *Endothelial cell coverage in BRS and DES. Left: scanning electron microscopy of BRS (upper panel) and DES (lower panel) with higher magnification of boxed areas. Right: quantification of endothelial cells above stent struts.*

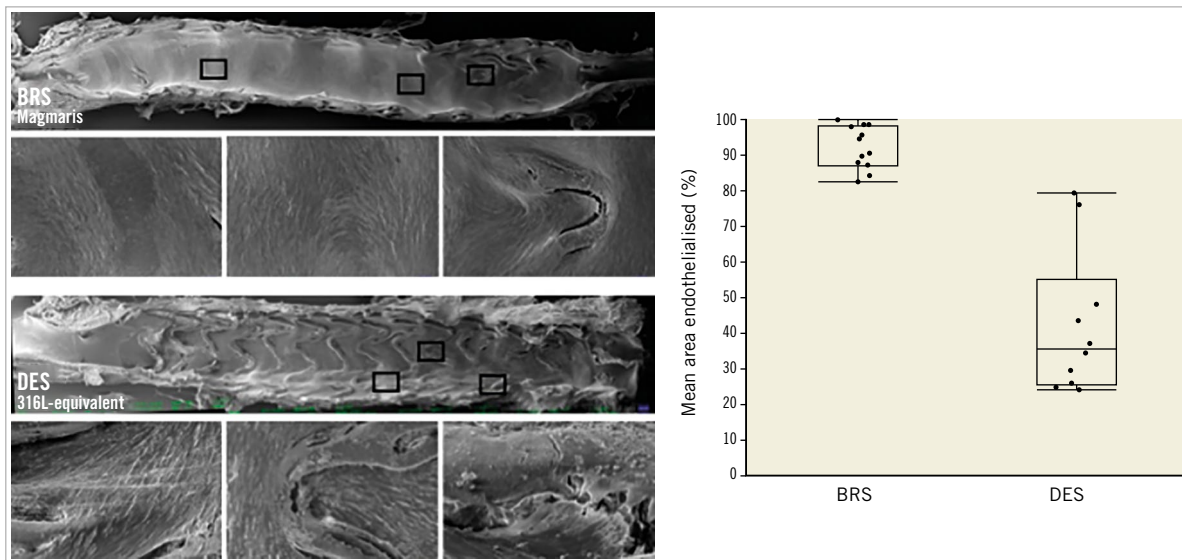Since reliable assessment of neoatherosclerosis by OCT alone remains controversial and prospective invasive imaging studies are challenging to perform, preclinical studies remain an important means to investigate the comparative effects of medical devices and pharmacological approaches in a timely manner. We have previously validated the currently applied animal model and found excellent agreement with regard to depiction of early signs of neoatherosclerosis such as foam cell infiltration within the nascent neointima following stent implantation[13]. Since early stages of neoatherosclerosis can be detected reliably by OCT (i.e., macrophage infiltration), the currently applied animal model holds great potential to gain a mechanistic understanding into the pathophysiology and adoption of therapeutic strategies for the treatment of neoatherosclerosis. The application of two distinct scoring systems for detecting neoatherosclerosis could have biased our results, especially when detecting neoatherosclerosis by OCT. However, reproducibility was satisfactory and variability rather low in both scores.

Owing to the inherent design constraints of the current animal study, absolute effect size in reducing neoatherosclerosis among BRS versus DES and atorvastatin versus placebo-treated animals is difficult to ascertain. This is also reflected by significant statistical interaction among these treatment approaches with regard to reduction of neointimal macrophages. It can therefore be assumed that BRS and atorvastatin therapy resulted in synergistic effects with regard to neoatherosclerosis progression over time, resulting in reduced neointimal macrophage infiltration.

Bioresorbable scaffold technology has recently suffered a major setback after the release of randomised controlled clinical trial data, which showed significantly increased revascularisation and device thrombosis rates at longer-term follow-up in broad patient subsets[14,15]. Potential mechanisms of late scaffold failure have been investigated in dedicated registries using OCT evaluating the long-term outcomes of polymeric BRS to delineate vascular morphology. These suggested late strut discontinuities, malapposition, neoatherosclerosis and underexpansion of the scaffold segment to be causally associated[16]. While most of these findings can be attributed to scaffold dismantling over time, neoatherosclerosis is not specifically linked to bioresorbable scaffold technology, and was indeed forecast to be erased with the use of BRS.

In our study, we observed decreased foam cell infiltration after implantation of magnesium-based BRS relative to a thick-strut permanent metallic DES, which may be secondary to accelerated vascular restoration (within six months) after magnesium-based BRS implantation relative to the three-year time frame observed with first-generation polymeric BRS, return to physiologic flow conditions and accelerated recovery of functional endothelial barrier function. Drug-induced impaired re-endothelialisation is likely to play a key role in the development of neoatherosclerosis as it allows the passage of inflammatory cells and lipoproteins into the developing neointima[17]. Quantitative evaluation of re-endothelialisation after 28 days showed significantly improved endothelial cell coverage in BRS compared with thick-strut DES. However, the lack of sufficient evaluation of endothelial leakiness in our study is a limitation. Our data are also in contrast to previous work by Waksman showing a lower degree of endothelialisation 28 days following stent implantation[18]: the main difference to our study can be seen in the procedural methodology of balloon denudation and the usage of healthy versus atherosclerotic animals. Most importantly, re-endothelialisation following arterial denudation is variable and depends largely on animal species, diseased versus healthy vascular tissue conditions, and the degree of vascular injury performed prior to stent implantation. In the study by Waksman et al, standard semi-compliant balloon catheters were inflated at the target site of stent implantation in healthy rabbits to achieve endothelial denudation.

In the current study, we used 3 Fr Fogarty catheters, which were inflated and repeatedly pulled back (arterial embolectomy catheters) to cause endothelial denudation in atherosclerotic rabbits. In our experience, the latter methodology causes a greater degree of endothelial denudation and vascular injury. As a consequence of greater endothelial injury in our study, proliferation and migration of endothelial cells is also markedly increased, which may explain the enhanced rate of re-endothelialisation 28 days after stent implantation. However, it is important to mention that re-endothelialisation was assessed at day 35 in this animal model, a time point at which lacking endothelial integrity is likely to impact substantially on cholesterol uptake into neointimal tissue and, consequently, formation of foamy macrophages. The fact that we observed increased foamy macrophage infiltration in thick-strut DES relative to BRS further strengthens this hypothesis. Atorvastatin has previously been proven to result in decreased plaque formation in hypercholesterolaemic rabbits[19,20]. There is abundant evidence of its clinical efficacy from large randomised controlled trials[7]. Atorvastatin was found to result in a highly significant 72% decrease of iliac-femoral lesion size following balloon injury in hypercholesterolaemic rabbits, which was attributed mainly to a significant reduction of intimal macrophages[20]. In a similar vein, Herdeg et al found a significant reduction in intimal and medial proliferation as well as peri-strut inflammation after atorvastatin therapy and bare metal stent implantation[19], which is in line with the findings of our study, where atorvastatin therapy resulted in significantly decreased neointimal macrophage infiltration irrespective of stent type.

In our study, atorvastatin relative to placebo therapy resulted in significantly diminished progression of neointimal foam cell infiltration, which was independent from the underlying stent type.

Limitations

Firstly, animal models are never able to replicate fully all the features of certain pathologies, e.g., we only observed the early stages of neoatherosclerosis and no advanced stages such as necrotic core formation. Also, the formation of foam cells is artificially accelerated (e.g., repeat endothelial denudation) compared to human coronary atherosclerosis, which usually takes decades to develop and depends on additional important co-factors that cannot be reproduced in current animal models.

Secondly, OCT has limitations in the detection of neoatherosclerosis, as mentioned above. This can be challenging when using degrading stent struts as a hallmark to differentiate neointima from native intima in OCT and could have biased the results of neoatherosclerosis scoring. However, even after degradation, BRS struts could be reliably recognised in the majority of cases and helped to differentiate progression of atherosclerosis versus neoatherosclerosis. Additionally, the use of co-registered histology allowed reliable diagnosis of neoatherosclerosis. Thirdly, transferability of preclinical findings to a human disease state is difficult to ascertain even after applying diseased animal models.

Finally, the use of a thick-strut DES is a limitation since modern DES have much thinner struts; thus, comparison to contemporary DES used in clinical practice with respect to neoatherosclerosis remains unknown.

Consequently, the current study should be viewed as hypothesis-generating. Clinical trials designed specifically to address neoatherosclerosis formation over time are needed to confirm these findings.

Conclusion

This study is the first to suggest reduction of in-stent neoatherosclerosis in bioresorbable magnesium scaffolds compared to thick-strut DES. High-dose statin therapy may be an important secondary prevention measure in patients with confirmed neoatherosclerosis. Prospective randomised trials are needed to evaluate these preclinical findings.

Impact on daily practice

Neoatherosclerosis was reported to contribute substantially to late stent failure, mainly caused by in-stent restenosis and stent thrombosis beyond the first year after stent implantation. In the current study, we investigated a second-generation magnesium-based BRS with regard to formation of neoatherosclerosis in hypercholesterolaemic rabbits relative to its stainless steel equivalent DES and found significantly reduced foam cell formation as an early sign of neoatherosclerosis in magnesium-based BRS. Clinical studies with appropriately designed endpoints are required to confirm these promising results in man.

Conflict of interest statement

M. Haude reports personal fees for consulting from Biotronik, outside the submitted work. M. Joner reports grants from the ESC's "Grants for Medical Research Innovation", during the conduct of the study, personal fees for consulting from Biotronik and OrbusNeich, and personal fees from speaker fees from Biotronik, OrbusNeich, Boston Scientific, Medtronic, and AstraZeneca, outside the submitted work. The other authors have no conflicts of interest to declare.

References

1. Benjamin EJ, Blaha MJ, Chiuve SE, Cushman M, Das SR, Deo R, de Ferranti SD, Floyd J, Fornage M, Gillespie C, Isasi CR, Jiménez MC, Jordan LC, Judd SE, Lackland D, Lichtman JH, Lisabeth L, Liu S, Longenecker CT, Mackey RH, Matsushita K, Mozaffarian D, Mussolino ME, Nasir K, Neumar RW, Palaniappan L, Pandey DK, Thiagarajan RR, Reeves MJ, Ritchey M, Rodriguez CJ, Roth GA, Rosamond WD, Sasson C, Towfighi A, Tsao CW, Turner MB, Virani SS, Voeks JH, Willey JZ, Wilkins JT, Wu JH, Alger HM, Wong SS, Muntner P; American Heart Association Statistics Committee and Stroke Statistics Subcommittee. Heart Disease and Stroke Statistics-2017 Update: A Report From the American Heart Association. *Circulation.* 2017;135:e146-603.

2. Serruys PW, de Jaegere P, Kiemeneij F, Macaya C, Rutsch W, Heyndrickx G, Emanuelsson H, Marco J, Legrand V, Materne P. A comparison of balloon-

expandable-stent implantation with balloon angioplasty in patients with coronary artery disease. Benestent Study Group. *N Engl J Med.* 1994;331:489-95.

3. Joner M, Finn AV, Farb A, Mont EK, Kolodgie FD, Ladich E, Kutys R, Skorija K, Gold HK, Virmani R. Pathology of drug-eluting stents in humans: delayed healing and late thrombotic risk. *J Am Coll Cardiol.* 2006;48:193-202.

4. Nakazawa G, Otsuka F, Nakano M, Vorpahl M, Yazdani SK, Ladich E, Kolodgie FD, Finn AV, Virmani R. The pathology of neoatherosclerosis in human coronary implants bare-metal and drug-eluting stents. *J Am Coll Cardiol.* 2011;57:1314-22.

5. Ali ZA, Serruys PW, Kimura T, Gao R, Ellis SG, Kereiakes DJ, Onuma Y, Simonton C, Zhang Z, Stone GW. 2-year outcomes with the Absorb bioresorbable scaffold for treatment of coronary artery disease: a systematic review and meta-analysis of seven randomised trials with an individual patient data substudy. *Lancet.* 2017;390:760-72.

6. Onuma Y, Muramatsu T, Kharlamov A, Serruys PW. Freeing the vessel from metallic cage: what can we achieve with bioresorbable vascular scaffolds? *Cardiovasc Interv Ther.* 2012;27:141-54.

7. Cannon CP, Braunwald E, McCabe CH, Rader DJ, Rouleau JL, Belder R, Joyal SV, Hill KA, Pfeffer MA, Skene AM; Pravastatin or Atorvastatin Evaluation and Infection Therapy-Thrombolysis in Myocardial Infarction 22 Investigators. Intensive versus moderate lipid lowering with statins after acute coronary syndromes. *N Engl J Med.* 2004;350:1495-504.

8. Nakazawa G, Vorpahl M, Finn AV, Narula J, Virmani R. One step forward and two steps back with drug-eluting-stents: from preventing restenosis to causing late thrombosis and nouveau atherosclerosis. *JACC Cardiovasc Imaging.* 2009;2:625-8.

9. Adriaenssens T, Joner M, Godschalk TC, Malik N, Alfonso F, Xhepa E, De Cock D, Komukai K, Tada T, Cuesta J, Sirbu V, Feldman LJ, Neumann FJ, Goodall AH, Heestermans T, Buysschaert I, Hlinomaz O, Belmans A, Desmet W, Ten Berg JM, Gershlick AH, Massberg S, Kastrati A, Guagliumi G, Byrne RA; Prevention of Late Stent Thrombosis by an Interdisciplinary Global European Effort (PRESTIGE) Investigators. Optical Coherence Tomography Findings in Patients With Coronary Stent Thrombosis: A Report of the PRESTIGE Consortium (Prevention of Late Stent Thrombosis by an Interdisciplinary Global European Effort). *Circulation.* 2017;136:1007-21.

10. Nakano M, Otsuka F, Yahagi K, Sakakura K, Kutys R, Ladich ER, Finn AV, Kolodgie FD, Virmani R. Human autopsy study of drug-eluting stents restenosis: histomorphological predictors and neointimal characteristics. *Eur Heart J.* 2013;34:3304-13.

11. Williams KJ, Tabas I. The response-to-retention hypothesis of early atherogenesis. *Arterioscler Thromb Vasc Biol.* 1995;15:551-61.

12. Gada H, Kirtane AJ, Newman W, Sanz M, Hermiller JB, Mahaffey KW, Cutlip DE, Sudhir K, Hou L, Koo K, Stone GW. 5-year results of a randomized comparison of XIENCE V everolimus-eluting and TAXUS paclitaxel-eluting stents: final results from the SPIRIT III trial (clinical evaluation of the XIENCE V everolimus eluting coronary stent system in the treatment of patients with de novo native coronary artery lesions). *JACC Cardiovasc Interv.* 2013;6:1263-6.

13. Nicol P, Lutter C, Bulin A, Castellanos MI, Lenz T, Hoppmann P, Lahmann AL, Colleran R, Euller K, Steigerwald K, Neubauer S, Rechenmacher F, Ludwig BS, Weinmüller M, Kerch G, Guo L, Cheng Q, Joner M. Assessment of a pro-healing stent in an animal model of early neoatherosclerosis. *Sci Rep.* 2020;10:1-10.

14. Kereiakes DJ, Ellis SG, Metzger C, Caputo RP, Rizik DG, Teirstein PS, Litt MR, Kini A, Kabour A, Marx SO, Popma JJ, McGreevy R, Zhang Z, Simonton C, Stone GW; ABSORB III Investigators. 3-Year Clinical Outcomes With Everolimus-Eluting Bioresorbable Coronary Scaffolds: The ABSORB III Trial. *J Am Coll Cardiol.* 2017;70:2852-62.

15. Wykrzykowska JJ, Kraak RP, Hofma SH, van der Schaaf RJ, Arkenbout EK, IJsselmuiden AJ, Elias J, van Dongen IM, Tijssen RYG, Koch KT, Baan J Jr, Vis MM, de Winter RJ, Piek JJ, Tijssen JGP, Henriques JPS; AIDA Investigators. Bioresorbable Scaffolds versus Metallic Stents in Routine PCI. *N Engl J Med.* 2017;376:2319-28.

16. Yamaji K, Ueki Y, Souteyrand G, Daemen J, Wiebe J, Nef H, Adriaenssens T, Loh JP, Lattuca B, Wykrzykowska JJ, Gomez-Lara J, Timmers L, Motreff P, Hoppmann P, Abdel-Wahab M, Byrne RA, Meincke F, Boeder N, Honton B, O'Sullivan CJ, Ielasi A, Delarche N, Christ G, Lee JKT, Lee M, Amabile N, Karagiannis A, Windecker S, Räber L. Mechanisms of Very Late Bioresorbable Scaffold Thrombosis: The INVEST Registry. *J Am Coll Cardiol.* 2017;70: 2330-44.

17. Finn AV, Joner M, Nakazawa G, Kolodgie F, Newell J, John MC, Gold HK, Virmani R. Pathological correlates of late drug-eluting stent thrombosis: strut coverage as a marker of endothelialization. *Circulation.* 2007;115:2435-41.

18. Waksman R, Zumstein P, Pritsch M, Wittchow E, Haude M, Lapointe-Corriveau C, Leclerc G, Joner M. Second-generation magnesium scaffold Magmaris: device design, and preclinical evaluation in a porcine coronary artery model. *EuroIntervention.* 2017;13:440-9.

19. Herdeg C, Fitzke M, Oberhoff M, Baumbach A, Schroeder S, Karsch KR. Effects of atorvastatin on in-stent stenosis in normo- and hypercholesterolemic rabbits. *Int J Cardiol.* 2003;91:59-69.

20. Bocan TMA, Mazur MJ, Bak Mueller S, Brown EQ, Sliskovic DR, O'Brien PM, Creswell MW, Lee H, Uhlendorf PD, Roth BD, et al. Antiatherosclerotic activity of inhibitors of 3-hydroxy-3-methylglutaryl coenzyme A reductase in cholesterol-fed rabbits: a biochemical and morphological evaluation. *Atherosclerosis.* 1994;111:127-42.

21. Joner M, Farb A, Cheng Q, Finn AV, Acampado E, Burke AP, Skorija K, Creighton W, Kolodgie FD, Gold HK, Virmani R. Pioglitazone inhibits in-stent restenosis in atherosclerotic rabbits by targeting transforming growth factor-beta and MCP-1. *Arterioscler Thromb Vasc Biol.* 2007;27:182-9.

22. Malle C, Tada T, Steigerwald K, Ughi GJ, Schuster T, Nakano M, Massberg S, Jehle J, Guagliumi G, Kastrati A, Virmani R, Byrne RA, Joner M. Tissue characterization after drug-eluting stent implantation using optical coherence tomography. *Arterioscler Thromb Vasc Biol.* 2013;33:1376-83.

23. Schwartz RS, Huber KC, Murphy JG, Edwards WD, Camrud AR, Vlietstra RE, Holmes DR. Restenosis and the proportional neointimal response to coronary artery injury: results in a porcine model. *J Am Coll Cardiol.* 1992; 19:267-74.

24. Otsuka F, Vorpahl M, Nakano M, Foerst J, Newell JB, Sakakura K, Kutys R, Ladich E, Finn AV, Kolodgie FD, Virmani R. Pathology of second-generation everolimus-eluting stents versus first-generation sirolimus- and paclitaxel-eluting stents in humans. *Circulation.* 2014;129:211-23.

25. Nakano M, Vorpahl M, Otsuka F, Taniwaki M, Yazdani SK, Finn AV, Ladich ER, Kolodgie FD, Virmani R. Ex vivo assessment of vascular response to coronary stents by optical frequency domain imaging. *JACC Cardiovasc Imaging.* 2012;5:71-82.

Supplementary data

Supplementary Appendix 1. Methods.

Supplementary Appendix 2. Results.

Supplementary Figure 1. Serum cholesterol levels.

Supplementary Table 1. Overview of results from histopathological analysis of group 1 (n=9 rabbits) after 91 days.

Supplementary Table 2. Overview of results from OCT analysis of group 1 (n=9 rabbits) after 91 days.

Supplementary Table 3. Additional results from histopathological analysis of groups 2 and 3 (n=10 rabbits each) after 161 days.

Supplementary Table 4. Additional results from OCT analysis of groups 2 and 3 (n=10 rabbits each) after 161 days.

Supplementary data

Supplementary Appendix 1. Methods

Study flow

Animals assigned to histology and optical coherence tomography

In a total of 33 rabbits, one BRS (n=33) and one permanent metallic DES (n=33) of equivalent geometry and design were randomly allocated to implantation into the right and left iliac arteries, respectively. Twenty-two rabbits were randomised to statin treatment (n=11, group 2) or placebo (n=11, group 3), while another 11 rabbits were terminated after 91 days (n=11, group 1) for evaluation of neoatherosclerosis formation prior to receiving statin therapy. All animals were fed a high-cholesterol diet (1% for 35 days followed by 0.025% until day 161). After seven days, endothelial balloon injury of the iliac arteries was performed using a Fogarty catheter, as previously described [21], followed by implantation of BRS and DES in accordance with random assignment. After 63 days, repeat balloon injury of the stented segment was performed to accelerate neoatherosclerosis formation. Animals of group 1 were terminated after 91 days while animals of groups 2 and 3 (n=11 each) were started on high-dose statin therapy (atorvastatin 3 mg/kg/d) or placebo and terminated after 161 days **(Figure 1)**.

Animals assigned to scanning electron microscopy

Endothelialisation was investigated by scanning electron microscopy (SEM) in 12 rabbits (12 BRS and 12 DES) 28 days following stent implantation (day 35). Animals were fed an hypercholesterolaemic diet (1% cholesterol) throughout the entire in-life phase **(Figure 1)**.

Study devices

In this study, a fully bioresorbable magnesium scaffold (Magmaris®; Biotronik AG, Bülach, Switzerland) was compared with a custom-designed 316L stainless steel drug-eluting stent (Biotronik AG) of equivalent geometry and design. Both BRS and DES were of the same size (3.0x15 mm), had a 6 crown 2 link design with a strut thickness of 150 µm and used PLLA coating to elute sirolimus at a concentration of 140 µg/cm².

Animal model of neoatherosclerosis

The rabbit model was approved by the government ("Regierung von Oberbayern", file number 55.2.1.54-2532-40-16) and was in accordance with the German Animal Welfare Act (version May 18, 2006, amended on March 29, 2017) as well as directive 2010/63/EU of the European Parliament on the protection of animals used for scientific purposes. Forty-five (45) New Zealand White rabbits (3.0 to 4.0 kg, 3 to 4 months of age; Charles River, France) were used for this preclinical animal model of in-stent neoatherosclerosis which has previously been established at our institution [13]. Animals were fed a 1% cholesterol diet (Altromin Spezialfutter GmbH, Lage, Germany) for seven days prior to balloon denudation of the iliac arteries, followed by stent implantation. After another four weeks of a high-cholesterol diet (1%), animals were switched to a 0.025% cholesterol diet (Altromin Spezialfutter GmbH) at day 35 and were continued on this diet until euthanasia. Blood samples were drawn on day 0, 7, 35, 63, 91, 126 and 161 for measurement of serum cholesterol and liver enzymes. Routine health checks including documentation of animal weight were performed three times a week.

Stent implantation, drug treatment, tissue harvest

On day 7, balloon denudation of the iliac arteries was performed using a 3 Fr Fogarty catheter before stents (3.0x15 mm; Biotronik AG) were implanted under fluoroscopic guidance at a nominal pressure of 10 atm (Magmaris) or 12 atm (316L SS-DES; Biotronik AG). Following implantation, vessel patency was documented by angiography. Animals received acetylsalicylic acid daily (40 mg/d) until the end of the experiment. Additionally, heparin (150 IU/kg) was administered during the procedure. On day 63, repeat denudation was performed to accelerate neoatherosclerosis formation. Animals assigned to SEM did not undergo repeat denudation procedures. Animals received buprenorphine (0.01 mg/kg) for a minimum of 24 hours after the interventions for post-procedural analgesia. On day 91, a subset of animals (n=11) was terminated to determine the magnitude of neoatherosclerosis formation prior to randomisation to statin treatment or placebo. The remaining animals (n=22) were randomised to statin (Atorvastatin Hennig® 10 mg) treatment (n=11) at an established dose of 3 mg/kg/d 10 per os or placebo (tap water per os) (n=11) and housed until day 161 to investigate changes in neoatherosclerosis progression over time. Euthanasia was induced by an overdose of pentobarbital, while rabbits were in deep anaesthesia. OCT imaging was performed immediately after euthanasia. Afterwards, iliac arteries were perfusion-fixed before they were processed for histopathological and immunohistochemical staining.

Histopathological and immunohistochemical processing

Stented arteries were embedded in methyl methacrylate (MMA). A total of five in-stent sections (10 µm thickness) were cut from each artery using a laser microtome (TissueSurgeon; LLS ROWIAK LaserLabSolutions GmbH, Hannover, Germany) and subsequently stained with haematoxylin-eosin (H&E) and Verhoeff-van Giesson (VVG). For immunohistochemistry, sections were stained using rabbit-specific antibodies against RAM-11 (Dako, Glostrup, Denmark, dilution 1:100) and SMA (Sigma Aldrich, St. Louis, MO, USA, dilution 1:150). Dako EnVision™ Mouse Secondary Antibody kit was used. Staining was performed using a fully automated stainer (Leica Bond RXm; Leica Biosystems Nussloch GmbH, Nussloch, Germany).

Scanning electron microscopy

Twenty-eight days following stent implantation (day 35), 12 animals were terminated for evaluation of endothelial cell coverage by SEM. Tissue was harvested as described above. The samples were then dehydrated in a graded series of ethanol, critical point dried, and sputter-coated with gold. Vessels were visualised using a scanning electron microscope (EVO MA 15; Carl Zeiss, Oberkochen, Germany). Endothelial cells were identified as sheets of spindle or polygon-shaped monolayers in close apposition, a distinguishing feature in contrast to other cell types in en face preparations. Quantification of endothelial coverage was achieved with the help of a customised software algorithm (ImageJ 1.5; NIH, Bethesda, MD, USA). Strut endothelialisation was derived from the total area of endothelialisation minus the area between stent struts.

Histopathological assessment

Morphometric measurements were performed in VVG-stained slides, as previously described [22]. In H&E-stained slides, giant cell infiltration, haemorrhage and mineralisation were evaluated and expressed as percentage, i.e., (% giant cells = number of struts with giant cells/number of struts in cross-section x100). Furthermore, injury of the vessel wall was scored according to the Schwartz method [23] and inflammation was analysed according to the scoring system established by Otsuka et al [24]. Final average values per vessel were derived from all five in-stent sections.

Neoatherosclerosis score in histology

Infiltration of foamy macrophages was assessed in histologic sections using a dedicated scoring system. Infiltration of foamy macrophages was assessed in histologic sections after H&E staining using a quadrant-based scoring system comprising the depth of foam cell infiltration into the neointimal tissue along the vascular circumference - score 1: no foamy macrophage infiltration; score 2: foamy macrophage infiltration in superficial tissue layers; score 3: foamy macrophage infiltration in deeper tissue layers; score 4: foamy macrophages in both superficial and deeper tissue layers. Mean values per cross-section were derived from individual data points at each quadrant. Final average score per vessel was derived from all five in-stent sections.

OCT imaging, neoatherosclerosis scoring and morphometric analysis

Optical coherence tomography (OCT) was performed immediately after euthanasia using the frequency-domain C7-XR™ OCT imaging console (OCT Intravascular Imaging System; St. Jude Medical, St. Paul, MN, USA). Image analysis was performed as previously described [22] using offline analysis (QIvus® Research Edition 3.0.26.0; Medis medical imaging systems bv, Leiden, the Netherlands). Analysis of OCT pullbacks included morphometric assessment of vessel dimensions and assessment of macrophage infiltration using an ordinal score.

For neoatherosclerosis scoring, OCT frames were evaluated for the presence of infiltrating macrophages with significant light attenuation [25] as well as hypo-intense areas with adjoining light attenuation. In every frame, the extent of infiltrating macrophages into the neointimal tissue was scored semi-quantitatively relative to the circumference of the vessel using an ordinal score - score 1: no macrophage infiltration; score 2: macrophage infiltration in <25% of the circumference; score 3: macrophage infiltration in 25-50% of the circumference; score 4: macrophage infiltration in 50-75% of the circumference; score 5: macrophage infiltration in >75% of the circumference. Final average score per vessel was derived from all in-stent OCT frames.

Morphometric measurements included lumen area, stent area and neointimal thickness over

struts. Neointimal area (stent area - lumen area) as well as percentage stenosis ([(stent area - lumen area)/stent area] x100) were calculated. Final average values per vessel were derived from every fifth in-stent OCT frame.

Statistical analysis

Continuous data are reported as mean with standard deviation in case of normal distribution and as median with interquartile range in case of non-parametric distribution. Distribution of data was confirmed by the Shapiro-Wilk goodness-of-fit test. The Wilcoxon Kruskal-Wallis rank-sum test was used to calculate the significance of differences between medians of non-parametric data, while ANOVA was used for group comparison of parametric data. To account for the clustered nature of data and the interaction of treatment assignments (BRS and DES assigned to statin and placebo), generalised estimating equation (GEE) modelling was used. For parametric data a linear model and for non-parametric data a gamma regression model with log link function was applied. Results are presented as estimated means with lower and upper 95% confidence interval (CI). To assess effects among local (BRS/DES) and systemic (statin/placebo) treatment, a p for interaction was calculated. To account for the categorical nature of the neoatherosclerosis score, Pearson's chi-square was also calculated for the quadrant-level comparison among treatment groups. Variability of scoring systems was calculated with intraobserver and interobserver correlation coefficients (ICCs) for absolute agreement. A p-value of $p<0.05$ was considered statistically significant. All analyses were carried out using JMP software, version 12.0 (SAS Institute, Cary, NC, USA) and SPSS, Version 22.0 (IBM Corp., Armonk, NY, USA).

Supplementary Appendix 2. Results

Results of group 1

Histopathological assessment of group 1 showed advanced neointimal coverage of stent struts in BRS relative to DES (% uncovered struts: 0.77% vs 33.64%, p=0.02). Neointima was thicker, but decreased foam cell infiltration was observed in BRS compared to DES (neointimal area: 3.01 mm² vs 1.89 mm², p=0.003; neoatherosclerosis score: 1.18 vs 1.43, p=0.0188) **(Supplementary Table 1, Supplementary Table 2)**.

Supplementary Figure 1. Serum cholesterol levels.
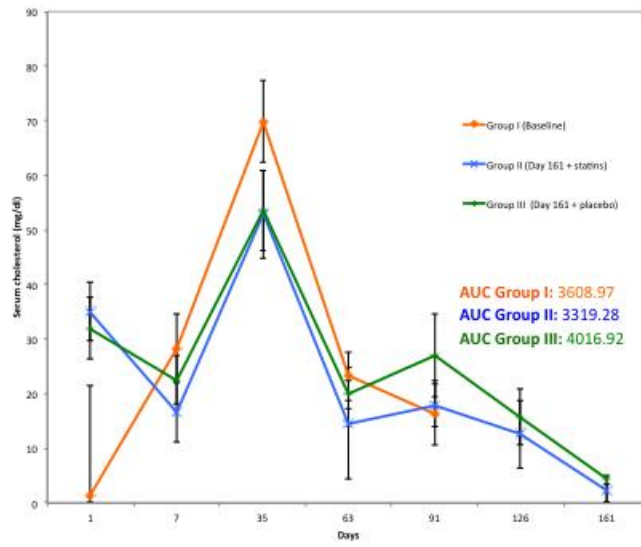
Supplementary Table 1. Overview of results from histopathological analysis of group 1 (n=9 rabbits) after 91 days.

		Area EEL [mm²]			Area IEL [mm²]		
		Mean	Std deviation	*p*-value	Mean	Std deviation	*p*-value
Treatment	**BRS, n=9**	5.58	0.58	0.0054*	5.26	0.56	0.0013*
	DES, n=9	6.44	0.55		6.26	0.53	
		Neointimal area [mm²]			Lumen area [mm²]		
		Mean	Std deviation	*p*-value	Mean	Std deviation	*p*-value
Treatment	**BRS, n=9**	3.01	0.59	0.0030*	2.24	0.72	0.0003*
	DES, n=9	1.89	0.76		4.37	0.70	
		Media area [mm²]			Injury score		
		Mean	Std deviation	*p*-value	Mean	Std deviation	*p*-value
Treatment	**BRS, n=9**	0.32	0.08	0.0005*	0.41	0.27	0.5660
	DES, n=9	0.18	0.04		0.48	0.27	
		Neoatherosclerosis score			Inflammation score		
		Mean	Std deviation	*p*-value	Mean	Std deviation	*p*-value
Treatment	**BRS, n=9**	1.18	0.08	0.0188*	1.84	0.76	0.1092
	DES, n=9	1.43	0.22		1.31	0.49	
		% Stenosis			% Uncovered struts		
		Mean	Std deviation	*p*-value	Mean	Std deviation	*p*-value
Treatment	**BRS, n=9**	58.21	11.25	0.0007*	0.77	1.59	0.0200*
	DES, n=9	30.07	10.63		33.64	27.88	

Values are presented as means with standard deviation. A p<0.05 was considered statistically significant (*).

Supplementary Table 2. Overview of results from OCT analysis of group 1 (n=9 rabbits) after 91 days.

		Lumen area [mm²]			Stent area [mm²]		
		Mean	Std deviation	*p*-value	Mean	Std deviation	*p*-value
Treatment	**BRS, n=9**	2.54	0.51	0.0013*	4.51	0.48	0.0017*
	DES, n=9	3.80	0.50		5.69	0.51	
		Neointimal area [mm²]			Neointimal thickness over struts [mm]		
		Mean	Std deviation	*p*-value	Mean	Std deviation	*p*-value
Treatment	**BRS, n=9**	1.86	0.58	0.0193*	0.33	0.10	0.0041*
	DES, n=9	1.09	0.64		0.16	0.08	
		% Stenosis			Neoatherosclerosis score		
		Mean	Std deviation	*p*-value	Mean	Std deviation	*p*-value
Treatment	**BRS, n=9**	43.27	14.10	0.0031*	1.13	0.18	0.123
	DES, n=9	18.94	10.81		1.32	0.32	

Values are presented as means with standard deviation. A p<0.05 was considered statistically significant (*).

Supplementary Table 3. Additional results from histopathological analysis of groups 2 and 3 (n=10 rabbits each) after 161 days.

		Area EEL [mm²]					Area IEL [mm²]				
		Mean	Lower 95% CI	Upper 95% CI	*p*-value	B-value	Mean	Lower 95% CI	Upper 95% CI	*p*-value	B-value
Treatment	**BRS, n=10**	4.92	4.69	5.16	0.0001*	-0.282	4.69	4.46	4.93	0.0001*	-0.307
	DES, n=10	6.55	6.42	6.68			6.37	6.24	6.50		
Group	**Statin, n=10**	5.63	5.38	5.89	0.616	-0.011	5.42	5.17	5.69	0.624	-0.016
	Placebo, n=10	5.72	5.49	5.96			5.51	5.27	5.75		
p for interaction		0.828					0.994				

		Neointimal area [mm²]					Lumen area [mm²]				
		Mean	Lower 95% CI	Upper 95% CI	*p*-value	B-value	Mean	Lower 95% CI	Upper 95% CI	*p*-value	B-value
Treatment	**BRS, n=10**	3.22	2.96	3.48	0.0001*	0.987	1.47	1.28	1.69	0.0001*	-1.041
	DES, n=10	2.27	2.04	2.50			4.10	3.91	4.30		
Group	**Statin, n=10**	2.72	2.34	3.10	0.851	-0.005	2.44	2.20	2.71	0.912	-0.024
	Placebo, n=10	2.77	2.51	3.03			2.46	2.17	2.80		
p for interaction		0.662					0.817				

		Media area [mm²]					% Uncovered struts				
		Mean	Lower 95% CI	Upper 95% CI	*p*-value	B-value	Mean	Lower 95% CI	Upper 95% CI	*p*-value	B-value
Treatment	**BRS, n=10**	0.23	0.21	0.25	0.0001*	0.078	0.00	0.00	0.00	0.0001*	-12.03
	DES, n=10	0.18	0.16	0.20			15.58	8.98	27.02		
Group	**Statin, n=10**	0.21	0.19	0.23	0.807	0.031	0.038	0.025	0.058	0.786	-0.153
	Placebo, n=10	0.20	0.18	0.23			0.041	0.029	0.059		
p for interaction		0.044					0.786				

		Inflammation score					% Giant cells				
		Mean	Lower 95% CI	Upper 95% CI	*p*-value	B-value	Mean	Lower 95% CI	Upper 95% CI	*p*-value	B-value
Treatment	**BRS, n=10**	1.53	1.31	1.75	0.106	-0.057	9.33	6.76	11.90	0.335	0.574
	DES, n=10	1.24	1.01	1.47			7.70	5.92	9.47		
Group	**Statin, n=10**	1.46	1.27	1.65	0.293	-0.200	8.90	6.65	11.15	0.601	-0.284
	Placebo, n=10	1.31	1.11	1.51			8.13	6.29	9.96		
p for interaction		0.054					0.786				

		Injury score									
		Mean	Lower 95% CI	Upper 95% CI	*p*-value	B-value					

Treatment	**BRS, n=10**	0.40	0.35	0.45	0.776	-0.046					
	DES, n=10	0.42	0.34	0.49							
Group	**Statin, n=10**	0.43	0.36	0.51	0.311	0.014					
	Placebo, n=10	0.39	0.34	0.44							
***p* for interaction**		0.426									

Values are presented as estimated means with upper and lower 95% CI. A p<0.05 was considered statistically significant (*).

Supplementary Table 4. Additional results from OCT analysis of groups 2 and 3 (n=10 rabbits each) after 161 days.

		Lumen area [mm²]					Stent area [mm²]				
		Mean	Lower 95% CI	Upper 95% CI	*p*-value	B-value	Mean	Lower 95% CI	Upper 95% CI	*p*-value	B-value
Treatment	**BRS, n=10**	2.08	1.81	2.39	0.0001*	-0.875	4.08	3.75	4.44	0.0001*	-0.412
	DES, n=10	4.61	4.41	4.82			5.97	5.82	6.12		
Group	**Statin, n=10**	3.16	2.89	3.45	0.596	-0.038	4.99	4.70	5.29	0.660	-0.009
	Placebo, n=10	3.04	2.70	3.41			4.88	4.52	5.28		
p for interaction		0.302					0.422				
		Neointimal area [mm²]					Neointimal thickness over struts [mm]				
		Mean	Lower 95% CI	Upper 95% CI	*p*-value	B-value	Mean	Lower 95% CI	Upper 95% CI	*p*-value	B-value
Treatment	**BRS, n=10**	1.86	1.63	2.09	0.0001*	0.611	0.34	0.30	0.39	0.0001*	0.666
	DES, n=10	1.32	1.12	1.52			0.19	0.16	0.22		
Group	**Statin, n=10**	1.62	1.33	1.92	0.723	0.133	0.26	0.22	0.31	0.639	0.133
	Placebo, n=10	1.56	1.38	1.74			0.25	0.22	0.28		
p for interaction		0.587					0.327				

Values are presented as estimated means with upper and lower 95% CI. A p<0.05 was considered statistically significant (*).